

# Reports

## Multiple-Scale Convection in the Earth's Mantle: A Three-Dimensional Study

**Abstract.** *Laboratory experiments suggest that a convective regime characterized by two length scales of motion is a reasonable model for circulations in the earth's upper mantle. The flows of largest horizontal scale represent a likely plate-driving mechanism, required by some theories of plate tectonics. It is also suggested that the small-scale circulations could influence the chemical evolution of the mantle by extracting primitive mantle material that is otherwise entrained in the large-scale flow.*

A possible although controversial model for convection in the mantle limits the circulations that directly act on the lithospheric plates to a maximum depth of about 700 km (1). It is based on the occurrence of deep earthquakes in subduction zones which are interpreted as due to collisions between sinking lithospheric slabs and the boundary of a layer of much higher viscosity. Justification of this model is complicated by the role of buoyancy-driven circulations in maintaining the plate motions. It has been argued that a scale of motion comparable to the characteristic horizontal dimension of a plate is required to exert sufficient force on its base to offset retarding forces. However, most studies have shown that natural convection is characterized by a horizontal scale comparable to the depth of the convection zone—a scale that seems much too small for driving plates (2). The occurrence of convective motions on two very different horizontal scales is a possible solution that is supported by the results of some analytical and numerical studies (3, 4) and by results obtained in a recent laboratory investigation.

The laboratory model consists of an internally heated fluid layer with a top boundary at a nearly constant temperature and an insulating bottom (Fig. 1a). The experiment models the temperature distribution resulting from a uniform concentration of radioactive heat sources like those contributing to heat production within the upper mantle. The heat sources are simulated by the ohmic dissipation of an electric current passed through the electrolyte fluid layer. Care was taken to minimize the effects of nonuniform heating by placing the mesh

electrodes on the horizontal boundaries, which minimizes their separation distance, and an alternating current was applied to eliminate polarization effects in the fluid. Observations of the convective planform were made by using the shadowgraph method (5). A collimated light beam projected through the layer and then onto a frosted screen causes cool sinking regions to appear more intense than warm ascending flows. Time-lapse photography allowed the large-scale flow to be observed and permitted estimation of the flow rate.

Specification of the dimensionless groupings of parameters (6) called the Rayleigh number

$$Ra = \frac{\alpha g H d^3}{\nu \kappa^2 \rho C_p}$$

and the Prandtl number

$$Pr = \frac{\nu}{\kappa}$$

determine the convective state of the model. The initially static layer becomes thermally unstable and flows begin to develop when the Rayleigh number exceeds 2772 (7). The upper mantle Rayleigh number is estimated to be about  $10^6$ , while the Prandtl number for the mantle is usually taken to be infinite ( $> 10^{20}$ ). Comparable values of the Rayleigh number can be achieved in the experiment by using a glycerin-based solution having a Prandtl number of about 3000. This relatively low Prandtl number is still sufficiently large to ensure reasonable correspondence with an infinite Prandtl number model.

Figure 1b shows the convection layer viewed from above; the bright linear features are sinking sheets in the flow,

forming loosely defined convection cells. The warm flow rises in the center of the cells and is cooled by the top boundary as it moves toward the outside of the cells. Near the cell edges the boundary-layer flow becomes unstable and falls into the interior region. This behavior is observed in the range of Rayleigh number from  $1.0 \times 10^5$  to  $3.5 \times 10^5$ . Estimates of the distance from the edge to the center of these irregular cells yield values comparable to the depth.

However, an increase in the Rayleigh number to  $7 \times 10^5$  produces a significant modification of the planform, as is evident from Fig. 2a. The linear features rapidly break down into sinking jets or blobs of fluid, which fall away from the cool top boundary into the interior flow, where they eventually come into thermal equilibrium with their surroundings. These blobs also form spontaneously adjacent to the top boundary over the rising regions. The resulting scale of motion near the top is much smaller than the depth of the system. Nearly concurrent with the appearance of these small-scale circulations, a complicated flow having roll diameters of at least six times the depth of the tank can be observed in time-lapse films of the experiment (arrows indicate the approximate direction of flow in Fig. 2a). This large-scale flow, having a maximum velocity of  $10^{-2}$  cm/sec, tends to sweep the sinking blobs to the edges of the convection layer. During the circulation time of the larger component of the flow, blobs form and disappear many times at any particular location on the boundary. The schematic diagram of Fig. 2b illustrates both flows in cross section. The results suggest that the large-scale component of a similar two-scale system in the mantle can have a wavelength comparable to the dimensions of typical lithospheric plates.

Several possible models exist to explain the relation between the large and small scales of motion, but the observations strongly suggest a preference. It is observed that the small-scale sinking jets appear before any large-scale motion can develop; that is, large-scale circulations do not cause the breakdown of the linear features seen in Fig. 1b. Either the small-scale jets or blobs contribute to driving the larger scale of flow, or they are more conducive than the original planform to allowing the large circulations to be driven by some other means, most likely the loss of heat to the sidewalls of the tank.

While the jets probably are less effective than the larger cells in preventing the development of large-scale circulation, it seems unlikely that sidewall cooling is the driving mechanism for the

larger circulations. In the experiment, the 1.3-cm-thick Plexiglas walls should be nearly adiabatic, since they have been placed in contact on their outer side with a 15-cm-wide region of fluid heated internally at the same rate as the fluid in the observation region. Results of an investigation (8) of the effect of sidewall heat fluxes on driving large circulations can be used to infer that heat losses in the present experiment are much too small to drive the observed motions.

The jets themselves are most likely responsible for the large component of flow. Reynolds stresses produced by the falling jets have been suggested as a mechanism for driving some large-scale flows (8). However, for a given Rayleigh number, the mechanism becomes less effective with increasing Prandtl number.

The Prandtl number of the experiment reported here is evidently too large for these flows to be explained by the production of Reynolds stresses. For the same reason, this theory is not expected to be relevant for mantle convection characterized by  $Pr > 10^{20}$ . Alternatively, baroclinicity caused by the jets falling into the interior can drive such flows, according to a two-dimensional numerical study carried out for an infinite Prandtl number fluid (4). The two-scale flow is associated with a constant heat flux condition on the upper boundary, modeling the earth's insulating lithosphere which overlies the convection zone. At large values of the Rayleigh number the insulating glass top of the experiment also approaches this thermal boundary condition (9).

The model presented here differs considerably from an earlier model of the interaction between two scales of convection in the mantle (10). In the development of that model, a more kinematic approach was taken regarding the processes that give rise to the two scales of motion. The larger component was presumed to be induced by the plate motions, so that a moving plate provided a constant-velocity boundary condition for the underlying fluid. The smaller scale of the flow, which resulted from thermal instability produced by bottom heating, was modeled by two-dimensional rolls having a vertical scale equal to the depth of the convection zone and an aspect ratio of about unity.

From the results presented here, it can be argued that the two scales of convection are an inherent property of the flows in the range of Rayleigh number considered. The larger scale does not depend on the existence of the appropriate kinematic boundary condition, that is, a moving boundary. The small component of the flow is likely to be three-dimensional and somewhat smaller in scale than the vertical dimension of the convection zone. Another feature of this internally heated model is that all the fluid from the interior of the convection zone is advected through the thermal boundary layer at the top. In the roll model, fluid will tend to be trapped in the interior of the convection roll in the absence of other transport processes. Such differences could be significant for geochemical models of the mantle.

The three-dimensional observations of convection in an internally heated layer described here complement the more general numerical models of Hewitt *et al.* (4). Their results suggest that the transition to two-scale convection is not very dependent on the mode of heating, rather it depends on the thermal boundary conditions. On the other hand, it may be inferred from the present observations that the restriction of their model to two dimensions and the implementation of less realistic stress-free boundary conditions have not introduced extraneous effects into their analysis. A future laboratory model might include heating from below as well as from within, which is undoubtedly a more accurate (and more complicated) model of the mantle. While the introduction of an unstable thermal boundary layer adjacent to the heated bottom would not be expected to strongly modify the two-scale behavior (4), the observations of the interaction between hot rising plumes produced in the unstable boundary layer and the large-scale flow would in themselves be interesting

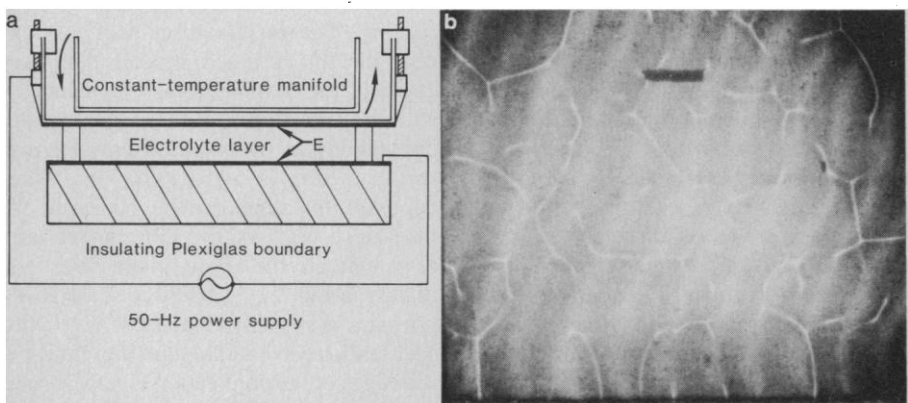


Fig. 1. (a) The top boundary of the convection layer is the base plate of a manifold constructed from plate glass over which thermostatically controlled water is circulated. The insulating bottom boundary consists of sheets of glass and Plexiglas. Copper mesh was chosen for the electrodes (E) to allow the passage through the layer of the light beam used to visualize the convection. The shadowgraph visualization technique is based on the dependence of the fluid's refractive index on temperature. (b) Observation made at a Rayleigh number of about  $3 \times 10^5$ . The flow is upward (out of the page) except near the bright linear features, which are sinking (into the page). The silhouetted scale near the top is 5 cm long, and the depth of the layer is 3 cm. The wavy moiré pattern observed in the photographs results from the projection of the light beam through both mesh electrodes. The pattern has no relation to the convection.

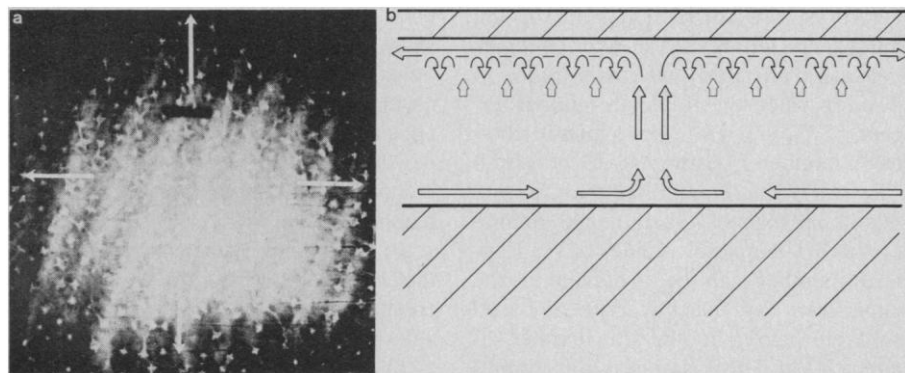


Fig. 2. (a) Observation made at a Rayleigh number of about  $7 \times 10^5$ . The linear features break down into sinking blobs or jets, their spacing decreasing with increasing Rayleigh number. A large-scale flow is also observed to develop nearly simultaneously with the jets. The jets act as particle tracers, allowing the flow to be mapped (arrows). (b) Schematic cross section of the two-scale flow, illustrating the large-scale upwelling of fluid near the center of the layer and the smaller scale sinking jets and return flow near the top boundary. The smaller scale of flow provides an efficient means of extracting fluid entrained in the larger component.

for studies of hot spots—regions on the earth's surface of intense intraplate volcanism.

CHARLES R. CARRIGAN\*

Department of Earth Sciences,  
Bullard Laboratories, Cambridge  
University, Cambridge, England, and  
Geophysical Research Division,  
Sandia National Laboratories,  
Albuquerque, New Mexico 87115

#### References and Notes

1. Convection below 700 km is not necessarily ruled out by this model since independent circulation systems could exist in the upper and lower mantle.
2. L. Knopoff, *Geophys. Monogr. Am. Geophys. Union* 13 (1969), pp. 683–689; D. J. Stevenson and J. S. Turner, in *Earth, Its Origin, Evolution and Structure*, M. McElhinny, Ed. (Academic Press, New York, 1979), pp. 227–263.
3. F. H. Busse and N. Riahi, *J. Fluid Mech.* 96, 243 (1980).
4. J. M. Hewitt, D. P. McKenzie, N. O. Weiss, *Earth Planet. Sci. Lett.* 51, 370 (1980).
5. M. M. Chen and J. Whitehead, *J. Fluid Mech.* 31, 1 (1968).

6. The symbols  $\alpha$ ,  $g$ ,  $H$ ,  $d$ ,  $C_p$ ,  $\nu$ ,  $\kappa$ , and  $\rho$  are, respectively, the volumetric coefficient of thermal expansion ( $4 \times 10^{-5} \text{ K}^{-1}$ ), the earth's gravitational acceleration ( $981 \text{ cm/sec}^2$ ), the volumetric heating rate ( $1.6 \times 10^{-16} \text{ cal/cm}^3\text{-sec}$ ), the depth of the convection layer ( $6 \times 10^7 \text{ cm}$ ), the specific heat ( $0.3 \text{ cal/g-K}$ ), the kinematic viscosity ( $10^{20} \text{ cm}^2/\text{sec}$ ), the thermal diffusivity ( $4 \times 10^{-3} \text{ cm}^2/\text{sec}$ ), and the density ( $4 \text{ g/cm}^3$ ). The numbers are appropriate for the values of these parameters in the mantle.
7. P. H. Roberts, *J. Fluid Mech.* 30, 33 (1967).
8. R. Krishnamurti and L. N. Howard, *Proc. Natl. Acad. Sci. U.S.A.* 78, 1981 (1981).
9. The Biot number based on the thickness of the thermal boundary layer is of order unity or less.
10. F. M. Richter and B. Parsons, *J. Geophys. Res.* 80, 2529 (1975).
11. I thank D. P. McKenzie for his suggestions and for providing support, financial and otherwise, during the laboratory phase of this study, which was carried out at Cambridge University, and D. Gubbins and J. A. Jacobs for helping to make possible my visit there. A United Kingdom Natural Environment Research Council grant and an NSF-administered NATO fellowship funded the work at Cambridge University. The work at Sandia National Laboratories was supported under DOE contract DE-AC04-76-DP00789.

\* Send reprint requests to Sandia National Laboratories, Albuquerque, N.M. 87115.

8 May 1981; revised 21 September 1981

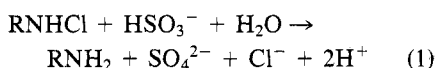
## Slowly Dechlorinated Organic Chloramines

**Abstract.** Dechlorination of some organic chloramines with aqueous sulfite solutions does not take place instantaneously as previously assumed. Field dechlorination times on the order of hours for some compounds that are found in chlorinated effluents appear likely on the basis of laboratory studies. These chlorinated compounds are not detected by standard analytical methods in the presence of sulfite ion.

Chlorinated effluents from electric power plants or sewage treatment plants have the potential to adversely affect the aquatic biota of the receiving water body (1). One approach to the control of chlorinated effluents is the use of chemical dechlorination, which usually consists of the addition of sulfur dioxide or sodium bisulfite ( $\text{NaHSO}_3$ ) to the effluent to degrade the oxidizing chlorine species to chloride ion. The conventional wisdom has held that, provided proper mixing is achieved, the reaction is quantitative and virtually instantaneous (2). We have found that at least some of the organic chloramines that form in chlorinated effluents react relatively slowly with aqueous  $\text{SO}_3^{2-}$  under environmentally meaningful conditions. Furthermore, with the present analytical techniques it is not possible to detect these compounds in the presence of excess unreacted dechlorinating agent. The extent and environmental significance of these slowly reacting compounds is presently unclear.

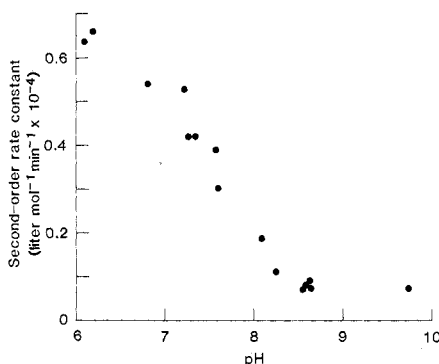
A significant proportion of the nitrogen compounds in many chlorinated effluents contain amino nitrogen groups. They are found in the *N*-terminal groups of amino acids and peptides, the amine nitrogens of peptides, and the alkyl

amine groups in the side chains of such amino acids as lysine (3). The *N*-terminal amino groups and the alkyl amines readily react with hypochlorous acid ( $\text{HOCl}$ ), formed by the hydrolysis of chlorine gas or sodium hypochlorite ( $\text{NaOCl}$ ), to give chloramines (4). In the course of studies of the reaction chemistry of these compounds, we found that at concentrations expected to be found in effluents ( $\sim 10^{-5}M$ ), the reaction



is relatively slow (R is an organic molecular fragment).

We have investigated the kinetics of Eq. 1, using several different organic



chloramines at 25°C. We followed the reactions by taking periodic aliquots of the reaction mixture and analyzing them according to the fluorescamine fluorometric method (5) to measure the concentration of the primary amines formed by the reaction of the chloramines with the aqueous  $\text{SO}_3^{2-}$ . This procedure is based on our observation that chloramines do not react with the fluorescamine reagent to form a fluorescent product. The fluorescence was measured with a fluorometer (Turner model 111). The reactions were carried out under conditions of excess  $\text{SO}_3^{2-}$  so that the reaction would obey pseudo-first-order kinetics. The monochloramine in all cases was formed by the reaction of the amine with an equimolar solution of  $\text{NaOCl}$  at concentrations of 3 to 11  $\mu\text{M}$  for 5 minutes. Sodium sulfite was then added to achieve an initial molar ratio to chloramine of from 3:1 to 30:1 in the reaction mixture. The pH was controlled with 0.02M phosphate buffers, and the temperature was regulated to  $\pm 0.1^\circ\text{C}$ .

If Eq. 1 is first order in the chloramine and in total  $\text{SO}_3^{2-}$ , the rate of appearance of the amine can be described by the equation

$$\frac{d[A]}{dt} = k[S][CLA] \quad (2)$$

where  $[A]$  is the concentration of the amine (in moles per liter),  $[S]$  is the concentration of total  $\text{SO}_3^{2-}$ ,  $[CLA]$  is the concentration of chloramine, and  $k$  is the rate constant (in liters per mole per minute). The solution of Eq. 2 under the assumptions of constant  $[S]$  and  $[CLA]_0 = [A]_t$  is

$$1 - \frac{[A]}{[A]_t} = \exp(-k[S]t) \quad (3)$$

where  $[CLA]_0$  is the initial concentration of chloramine and  $[A]_t$  is the sum of concentrations of chloramine and free amine. The pseudo-first-order rate constant ( $k' = k[S]$ ) can then be calculated using the method of least squares to fit the data on  $\ln(1 - [A]/[A]_0)$  versus time. We determined  $k'$  in this way for varying conditions of  $[A]_0$ ,  $[S]$ , and pH for the chloramine *N*-chloroalanylalanylalanine. The results showed that  $k'$  is independent of  $[A]_0$  and varies linearly with  $[S]$ . These results confirm the assumption that Eq. 1 is first order in  $[CLA]$  and  $[S]$ . The second-order rate constant is then obtained by dividing  $k'$  by  $[S]$ . Figure 1

Fig. 1. Second-order rate constant of the reaction of *N*-chloroalanylalanylalanine at 25°C as a function of pH.